Volume 7
Number 19
7 October 2025
Pages 5831–6274

# Nanoscale Advances

rsc.li/nanoscale-advances

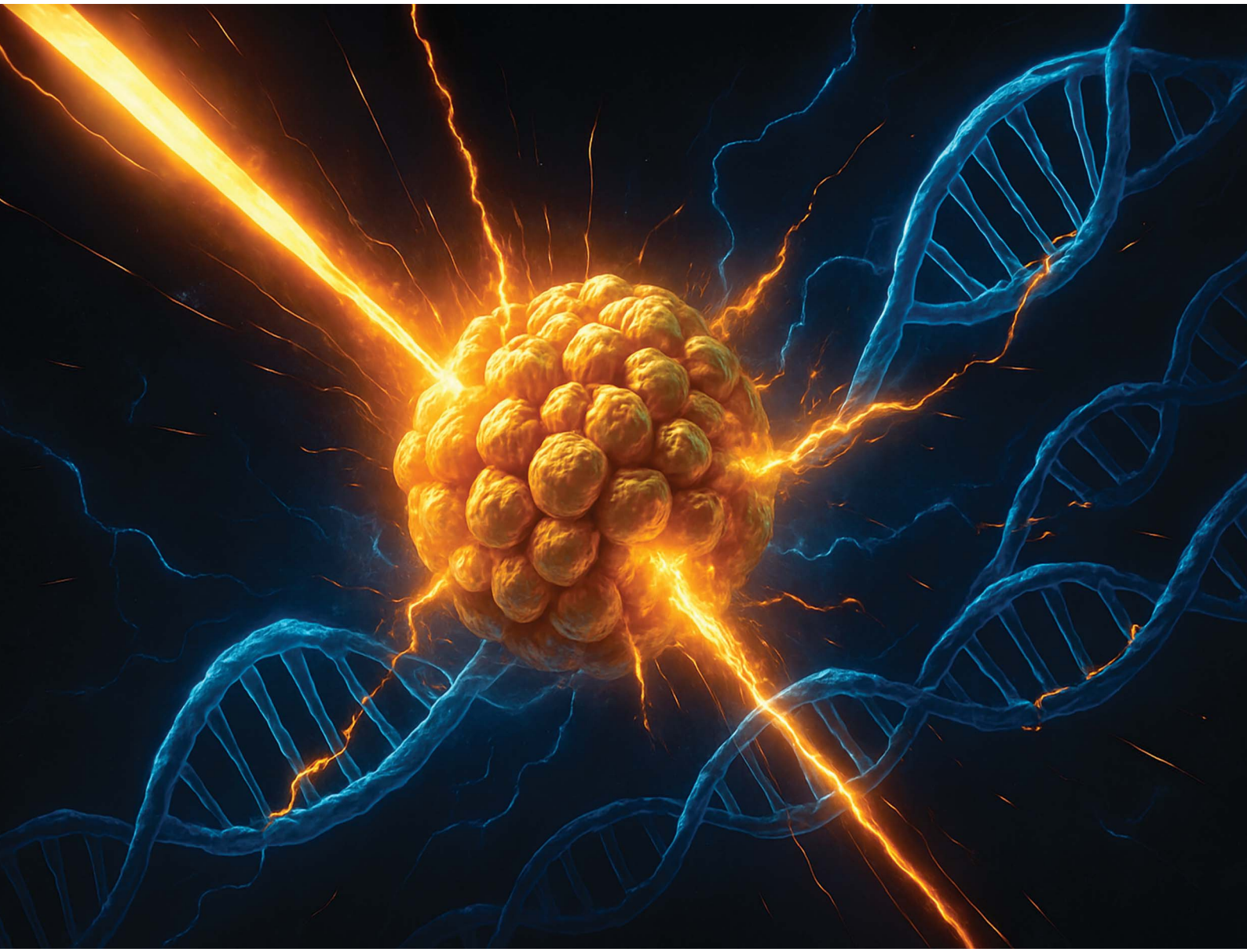

ISSN 2516-0230

ROYAL SOCIETY OF CHEMISTRY

**PAPER**

Shawn Wettig *et al.*

Engineered dual-functional gold nanoparticles enhance radiosensitization in prostate cancer cells: synergistic action of curcumin and gold

NCNST

Nanoscale Advances

ROYAL SOCIETY OF CHEMISTRY

PAPER

View Article Online
View Journal | View Issue



Cite this: *Nanoscale Adv.*, 2025, **7**, 5964

# Engineered dual-functional gold nanoparticles enhance radiosensitization in prostate cancer cells: synergistic action of curcumin and gold†

Mohamed Aborig, [a] Moad Alsefaou, [b] Ernest Osei [cef] and Shawn Wettig *[ad]

Prostate cancer remains a leading cause of cancer-related mortality in men, with the three main treatment modalities being surgery, chemotherapy, radiotherapy, or a combination depending on the stage. However, the use of radiotherapy is often restricted by dose-limiting toxicity of the organs at risk. To address this challenge, we developed curcumin-coated gold nanoparticles (Curc-GNPs) that leverage both the photoelectric properties of gold and the radiosensitizing effects of curcumin. In this study, we explore the stability, cytotoxicity, cellular uptake, and radio-sensitizing potential of Curc-GNP in PC-3 prostate cancer cells. Curc-GNPs exhibited a biphasic dose–response curve where concentrations up to 100 μg $mL^{-1}$ showed minimal cytotoxicity, whereas higher doses (>100 μg $mL^{-1}$) were markedly cytotoxic. Cellular uptake was enhanced under serum-free conditions. Clonogenic survival assays revealed significant radiosensitization (sensitizer enhancement ratio up to 1.82 at 500 μg per mL Curc-GNPs), linked to an elevated $\alpha$-parameter in the linear–quadratic model and heightened reactive oxygen species production. These results highlight Curc-GNPs as a promising platform for enhancing radiotherapy efficacy in prostate cancer while potentially mitigating off-target toxicity.

Received 18th April 2025
Accepted 4th July 2025

DOI: 10.1039/d5na00376h

rsc.li/nanoscale-advances



## 1. Introduction

Prostate cancer is the second leading cause of cancer-related mortality among American men, with approximately one in eight men diagnosed with the disease over the course of their lifetime.[1] Radiotherapy serves as a cornerstone in the management of medium- and high-risk prostate cancer, functioning as either a definitive treatment or as an adjuvant therapy in combination with postoperative care and/or hormonal therapy. The application of radiotherapy for patients with locally advanced prostate cancer has been associated with improved cancer-specific mortality and overall survival.[2] However, despite its effectiveness, the dose of radiotherapy is primarily constrained by the risk of radiation-induced toxicity to adjacent organs, particularly the rectum and bladder. This limitation has prompted extensive research into radiosensitizing agents aimed at enhancing the efficacy of radiotherapy in prostate cancer treatment while minimizing toxicity to the organs at risk.

Curcumin, a polyphenolic compound derived from turmeric, has attracted significant attention in cancer research due to its well-documented therapeutic properties, including anticancer, antioxidant, and anti-inflammatory effects.[3–7] Recent studies have demonstrated that curcumin can enhance the efficacy of radiotherapy across various cancer types, including prostate cancer, hepatocellular carcinoma, colorectal cancer, and glioblastoma.[8–10] One of the primary mechanisms by which curcumin enhances radiosensitivity is *via* the inhibition of the nuclear factor kappa B (NF-κB) signaling pathway, which is known to promote cell survival and resistance to apoptosis in response to radiation.[9] The modulation of NF-κB and cell cycle phase is a consistent finding across multiple studies, underscoring its important role in curcumin's potential to overcome radio-resistance in cancer cells.[3,4] However, free curcumin faces limitations such as poor aqueous solubility, low bioavailability, and rapid metabolism, which hinder its clinical application.

To address these challenges, researchers have incorporated curcumin into nanoparticle formulations to enhance its delivery and efficacy in cancer therapy. Among these agents, gold nanoparticles (GNPs) have attained considerable attention as one of the most extensively studied radiosensitizers owing to their unique physical and chemical properties including large surface area, *in vivo* biocompatibility, and easily modifiable surface.[11] The primary advantage of GNPs as radiosensitizers

[a]*School of Pharmacy, University of Waterloo, Kitchener, ON N2G 1C5, Canada. E-mail: maborig@uwaterloo.ca; wettig@uwaterloo.ca; Tel: +1-519-888-4567 (ext. 42221)*
[b]*Schulich School of Medicine & Dentistry, Western University, London, N6A 5C1, Ontario, Canada. E-mail: malsefao@uwo.ca*
[c]*Waterloo Regional Health Network Cancer Centre, Waterloo Regional Health Network at Midtown, Kitchener, ON N2G 1G3, Canada. E-mail: ernest.osei@whrn.ca*
[d]*Waterloo Institute for Nanotechnology, University of Waterloo, ON N2L 3G1, Canada*
[e]*Department of Systems Design Engineering, University of Waterloo, Waterloo, ON N2L 3G1, Canada*
[f]*Department of Physics and Astronomy, University of Waterloo, Waterloo, ON N2L 3G1, Canada*

† Electronic supplementary information (ESI) available. See DOI: https://doi.org/10.1039/d5na00376h

lies in their high atomic number, which facilitates increased photoelectric absorption and subsequent emission of secondary electrons and production of reactive oxygen species (ROS). These processes can damage nearby cancer cells, thereby enhancing the overall effectiveness of radiotherapy.[12,13]

In this study, we investigate the potential of curcumin-coated gold nanoparticles (Curc-GNPs) as a radiosensitizing agent for prostate cancer. Specifically, we assess their ability to enhance the efficacy of radiotherapy in PC-3 prostate cancer cells by leveraging the complementary mechanisms of GNPs and curcumin. The GNP platform is designed to improve curcumin's stability, bioavailability, and cellular uptake while simultaneously amplifying radiation-induced cytotoxicity through the generation of ROS and secondary electrons. Additionally, curcumin's inhibition of the NF-κB signaling pathway and G2/M cell cycle arrest may further enhance radiosensitivity by reducing cancer cell survival and promoting apoptosis.[3–5,9] To our knowledge, this is the first study to explore the combination of curcumin and GNPs as a radiosensitizing agent. By systematically investigating this nanoplatform, we aim to provide novel insights into the development of more effective radiosensitization strategies for high-risk prostate cancer, ultimately improving therapeutic outcomes while minimizing radiation-induced toxicity.

## 2. Materials and methods

### 2.1 Materials

Curcumin (≥98% purity, Alexis Biochemicals, San Diego, CA, USA), sodium citrate dihydrate (S25545-Fisher Scientific, Waltham, MA, USA), and gold(III) chloride trihydrate ($HAuCl_4 \cdot 3H_2O$, 520918-Aldrich, St. Louis, MO, USA) were used as supplied for the synthesis of GNPs. All synthesis protocols utilized ultrapure Milli-Q water derived from the Millipore Gradient A10 water purification system (Merck Millipore, MA, USA). Milli-Q water will be referred to as ultrapure water.

Reagents for *in vitro* studies included RPMI1640 medium (R8758 Aldrich), fetal bovine serum (FBS, A3160702 Fisher Scientific), penicillin streptomycin (PNC, 15140122 Fisher Scientific), Dulbecco's phosphate buffered saline (PBS, SH3002802 Fisher Scientific), trypsin–EDTA (25200072 Fisher Scientific), dimethyl sulfoxide (DMSO, MT25950CQC Fisher Scientific), and crystal violet (C0775100G Aldrich).

### 2.2 Synthesis and purification

The synthesis protocol for Curc-GNP was adapted from a procedure by Nambiar *et al.*[6] The first step involved solubilizing the polyphenol compound by adding 10 mM NaOH to a vial containing curcumin powder to form 10 mL of a 1 mM curcumin solution. The dark orange solution was then held in an ultrasonic bath at 44 °C, and 200 μL of 100 mM $HAuCl_4 \cdot 3H_2O$ was added dropwise. The formation of Curc-GNP was confirmed by the sudden change of the solution's color from orange to ruby red. The solution was transferred to a 3.5 kDa dialysis tubing (SnakeSkin Dialysis Tubing, Thermo Fisher, Waltham, MA, USA), which was then placed in a 2 L beaker of ultrapure water for ≥24 h.

The synthesis protocol for citrate-coated GNPs (Cit-GNP) followed the Turkevich method.[14] Briefly, 300 mL of 1 mM $HAuCl_4 \cdot 3H_2O$ stock solution was transferred to a round bottom flask, brought to a rolling boil, and refluxed. Subsequently, a 6 mL aliquot of 40 mM sodium citrate stock solution was added to the boiling $HAuCl_4 \cdot 3H_2O$ solution. During the reaction, the color of the solution gradually changed from yellow to brown and finally to ruby red. The final solution was then allowed to cool to room temperature with continuous stirring for 3 h followed by purifying it with 3.5 kDa dialysis tubing in a 2 L beaker of ultrapure water for ≥24 h.

### 2.3 Curc-GNP characterization

**2.3.1 Stability test.** The stability of CurcGNPs and Cit-GNPs was tested in ultrapure water, RPMI1640 (no additives), and serum-supplemented RPMI1640 (containing 10% v/v FBS and 1% v/v PNC). The samples were prepared in Petri dishes at the Au concentration of 100 μg $mL^{-1}$ in three medium conditions and incubated at 37 °C with 5% $CO_2$ for T = 0, 24, and 48 h. At each time point, 1 mL aliquot was transferred to a disposable cuvette to measure the hydrodynamic size, polydispersity index (PDI), and zeta potential using Malvern ZetaSizer UltraZS (Malvern Instruments Ltd., Malvern, UK). UV-vis absorbance spectra were obtained by a SpectraMax Molecular Devices M5 plate reader (San Jose, CA, USA). A single absorbance peak near 525 nm was used post synthesis to confirm the formation of spherical GNPs measuring approximately 15–30 nm in diameter.

**2.3.2 Transmission electron microscopy (TEM).** TEM images of Curc-GNPs were obtained using a Philips CM10 electron microscope. A few small drops of Curc-GNP were placed on a 200 mesh Formvar copper grid and left overnight to dry. TEM images were taken at an accelerating voltage of 60 kV, using a 100 nm scale bar. ImageJ software was used to analyze the size of the GNPs, and the Gaussian histogram for the size distribution of spherical Curc-GNPs was generated using Origin Pro software. Note that TEM size measurements represent only the diameter of the Au core, excluding the outer coating.

**2.3.3 Fourier transform infrared spectroscopy (FTIR).** FTIR spectroscopy was conducted to compare the characteristic absorption peaks of powdered curcumin (≥98% purity) with those of the freeze-dried Curc-GNPs. Analyses were performed on a Thermo Nexus 670 FTIR spectrometer equipped with a Continuum microscope, with spectra recorded in the solid state over the wavenumber range of 700–2500 $cm^{-1}$. Transmission peaks were examined to confirm the presence of curcumin on the gold nanoparticle surface and identify any shifts in functional group absorption relative to free curcumin.

**2.3.4 High performance liquid chromatography (HPLC).** Curcumin loading onto gold nanoparticles was quantified using a Waters Alliance HPLC system. Chromatographic separation was achieved on a C18 column using an isocratic mobile phase composed of aqueous 0.1% formic acid and 0.1% formic acid in acetonitrile (50 : 50, v/v) at a flow rate of 1.5 mL $min^{-1}$. Detection was carried out at 425 nm. A calibration curve was established using 6 curcumin standards (≥98% purity) at

concentrations of 0.1–54.25 μg $mL^{-1}$. To determine curcumin loading, curcumin was desorbed from the nanoparticle surface by treating the Curc-GNP suspension with acidified ethanol (0.1 mL formic acid per 100 mL ethanol). The mixture was sonicated, vortexed thoroughly, and centrifuged at 10 000×*g* for 10 minutes. The resulting supernatant was filtered through a 0.2 μm GHP syringe filter and analyzed *via* HPLC to determine the desorbed curcumin concentration. The GNP pellet was resuspended in acidified ethanol and the process was repeated again. Curcumin loading was calculated using the equation:

$$\omega_{\mathrm{Curc}} = \frac{m_{\mathrm{Curc}}}{m_{\mathrm{Au}}} \quad (1)$$

where $\omega_{\mathrm{Curc}}$ is the curcumin loading in mg Curc/mg Au, $m_{\mathrm{Curc}}$ is the desorbed curcumin content detected in the supernatant and $m_{\mathrm{Au}}$ is the mass of gold in the Curc-GNP suspension. Gold content was quantified by resuspending the nanoparticle pellet in ultrapure water and measuring the gold concentration using ICP-MS (Agilent Technologies).

**2.3.5 Antioxidant capacity of Curc-GNP.** The antioxidant potential of Curc-GNP and Cit-GNP was measured based on the (DPPH) 2,2-diphenyl-1-picrylhydrazyl radical scavenging assay adapted from Gülçin *et al.*,[15] whereby the antioxidant activity of a compound correlates with the spectrometric shift caused by DPPH reduction. Briefly, a 0.1 mM DPPH stock solution was prepared by dissolving 3.94 mg of DPPH powder in 100 mL ethanol. Four different concentrations (25, 50, 100, and 200 μg $mL^{-1}$) were tested for DPPH activity. 2 mL of each GNP solution was mixed with 2 mL of the DPPH stock solution, vortexed, and incubated in the dark for 30 minutes. Afterward, the samples were centrifuged at 3000 g for 10 minutes, and the supernatant was used for analysis. Absorbance was recorded at 517 nm on a Molecular Devices SpectraMax M5 plate reader. The absorbance readings were converted to antioxidant activity based on eqn (2):

$$\text{DPPH inhibition}(\%) = \left[\frac{\mathrm{Abs}_{\mathrm{control}} - \left(\mathrm{Abs}_{\mathrm{sample}} - \mathrm{Abs}_{\mathrm{blank}}\right)}{\mathrm{Abs}_{\mathrm{control}}}\right] \times 100\% \quad (2)$$

where $\mathrm{Abs}_{\mathrm{control}}$, $\mathrm{Abs}_{\mathrm{sample}}$, and $\mathrm{Abs}_{\mathrm{blank}}$ are the absorption readings of the DPPH control, the DPPH-treated samples, and the blank samples, respectively.

### 2.4 Cytotoxicity of Curc-GNP against PC-3 cells

The cytotoxicity of Curc-GNPs on prostate cancer cells (PC-3) was evaluated using a colorimetric XTT assay,[16] which detects the reduction of XTT to a soluble formazan product by metabolically active cells serving as an indicator of cell proliferation and viability. Briefly, PC-3 cells were seeded into 96-well plates at a density of 5000 cells per well and incubated in RPMI-1640 medium supplemented with 10% FBS and 1% PNC at 37 °C in a 5% $CO_2$ incubator for 24 hours to allow cell adherence and stabilization. Seven concentrations of Curc-GNPs (25, 50, 75, 100, 200, 500, and 1000 μg $mL^{-1}$) were prepared in serum-supplemented RPMI medium.

The negative control consisted of PC-3 cells incubated with cell medium only, whereas the blank control included cell medium plus Curc-GNPs without cells. Cells were exposed to each GNP concentration for treatment durations of 24, 48, and 72 hours. Each concentration and treatment time point was conducted in quintuplicate. At the end of each treatment time point, the medium was removed, and wells were gently rinsed twice with 100 μL PBS. Subsequently, 50 μL of XTT working solution was added to each well, and plates were incubated for an additional 4 hours. After incubation, absorbance was measured at 450 nm (reference: 650 nm) using a SpectraMax Molecular Devices M5 plate reader. Cell viability for each treatment group was calculated based on eqn (4), incorporating the specific absorbance calculated from eqn (3) to account for negative and blank controls. These results were used to determine the cytotoxic effects of each GNP structure in PC-3 cells at different concentrations and time points.

$$\text{Specific absorbance} = [\mathrm{Abs}_{450\ \mathrm{nm}}\ (\text{test}) - \mathrm{Abs}_{450\ \mathrm{nm}}\ (\text{blank})] - \mathrm{Abs}_{650\ \mathrm{nm}}\ (\text{test}) \quad (3)$$

$$\%\text{Viability} = \frac{\text{Specific Abs of treated wells}}{\text{Specific Abs of control}} \times 100 \quad (4)$$

$$\%\text{Cytotoxicity} = 100 - \%\text{Viability} \quad (5)$$

### 2.5 Cellular uptake of Curc-GNP using ICP-MS

Inductively coupled plasma-mass spectrometry (ICP-MS) can measure trace levels of elements in biological fluids. Here, the cellular uptake of Curc-GNP by PC-3 cells was quantified by measuring gold (Au) concentrations using ICP-MS (Agilent Technologies). The protocol, adapted from Carnovale *et al.*[17] examined the influence of incubation time (10 hours *vs.* 24 hours) and medium composition (serum-supplemented *vs.* non-serum-supplemented) on Curc-GNP uptake at two Au concentrations (50 and 100 μg $mL^{-1}$).[17] Briefly, PC-3 cells were seeded into six-well plates at a density of $3 \times 10^5$ cells per well in a growth medium. At 75% confluency, the medium was removed from each well and replaced with 3 mL of fresh medium containing 50 or 100 μg $mL^{-1}$ of Curc-GNPs. Cells were then incubated for 10 or 24 hours at 37 °C. Each concentration and condition were run in triplicate wells. After the designated incubation period, the medium was removed, and each well was gently washed three times with PBS to remove unbound GNPs. Cells were detached using 0.25% (w/v) trypsin, transferred to conical tubes for cell counting, and centrifuged at 500 g for 10 minutes. The supernatant was discarded, and the cell pellet was resuspended in ultrapure water and transferred to digestion tubes. 1 mL of aqua regia (1 : 3 $HNO_3$ : HCl) was added for acid digestion. The tubes were heated on a digestion block at 90 °C for 120 minutes. Afterward, each digest was diluted to 10 mL with ultrapure water and mixed thoroughly before Au analysis.

ICP-MS Analysis was performed for $^{197}Au$, with $^{89}Y$ serving as an internal standard to adjust for variations in plasma conditions. External calibration used a five-point calibration curve (1–100 ppm), and curve correlation coefficients were all >0.995. Calibration was verified against a separate 10 ppm or 50 ppm Au standard from a different source, with agreement within ±10%

 

of the expected value. The Method Detection Limit (MDL) and Limit of Quantification (LOQ) for gold in solution were 0.0408 ppm and 0.1300 ppm, respectively. The gold content per cell was calculated from ICP-MS data using eqn (6).

$$\text{Mass of Au per cell} = \frac{\text{ppm of Au detected by ICP}}{\text{Total cell count}} \quad (6)$$

### 2.6 *In vitro* radiosensitization analysis of Curc-GNP

Radiosensitization studies were performed using a clonogenic assay protocol (Fig. 1) adapted from Franken *et al.*[18] PC-3 cells were seeded in six-well plates at a density of $3 \times 10^5$ cells per well and grown to approximately 75% confluence. Subsequently, Curc-GNPs were administered at six different concentrations (0, 25, 50, 100, 200, and 500 μg $mL^{-1}$) and incubated for 24 hours.

Irradiation was conducted at the Waterloo Regional Health Network Cancer Centre using a Varian TrueBeam linear accelerator (Varian Medical Systems, Palo Alto, CA) with 6 MV X-rays at a 100 cm source-to-surface distance, calibrated according to AAPM TG-51 dosimetry protocol. The beam was collimated to a $20 \times 20$ $cm^2$ field for dose delivery of 2, 4, or 6 Gy. For each radiation dose, two six-well plates were used: one set for the treatment group (Curc-GNP + radiation) and another set for the control group (Curc-GNP only, no radiation). Each condition was performed in triplicate.

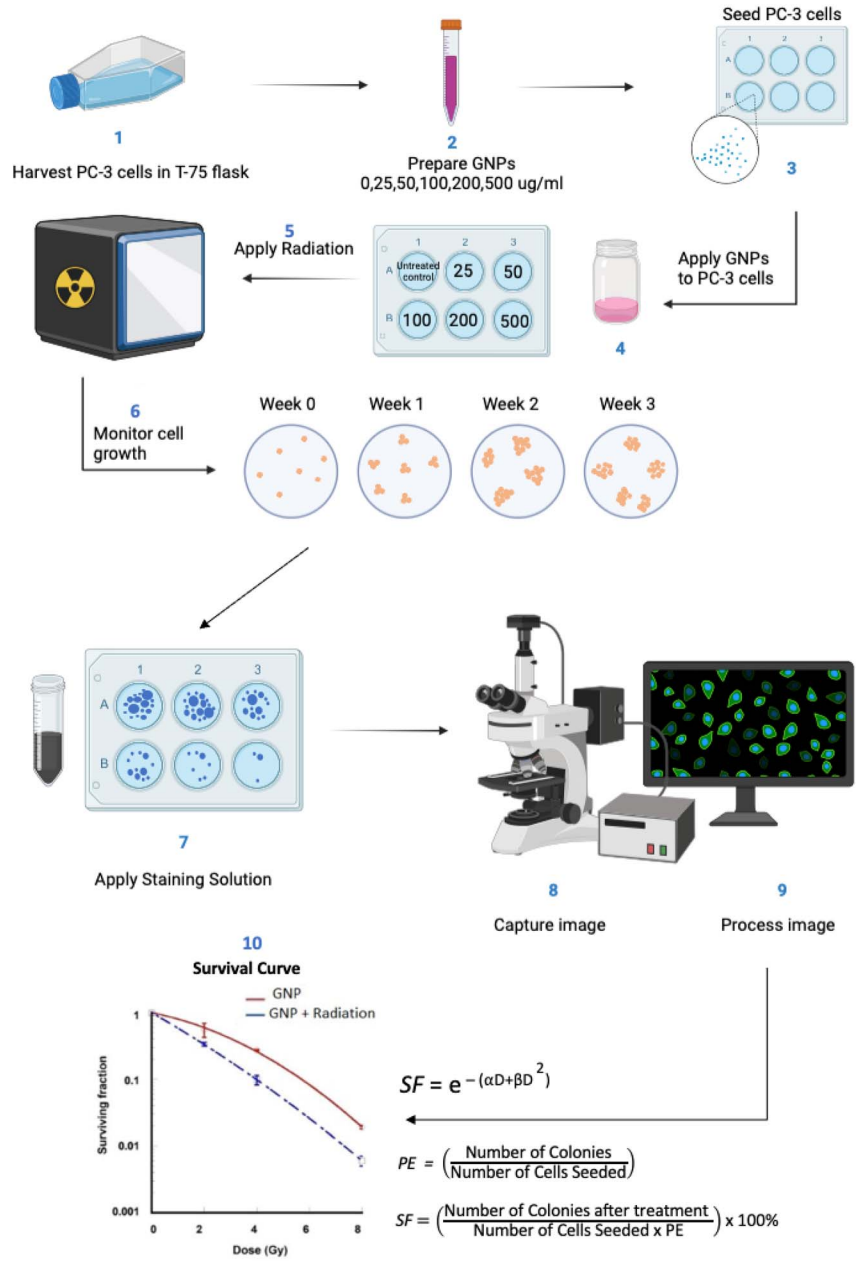


Fig. 1 A flow diagram showing the clonogenic assay protocol undertaken for measuring the radiation dose enhancement of Curc-GNP incubated with PC-3 cells.

Following irradiation, cells were washed with PBS, trypsinized, counted, and reseeded into new six-well plates. Colonies were allowed to form over a period of up to three weeks, with the endpoint determined when control wells showed sufficiently large, distinct colonies. Cells were stained with 0.4% crystal violet for 30 minutes, rinsed with deionized water, and dried overnight. Images of each well were taken and processed in ImageJ using the *ColonyCount* plugin to standardize colony counting and reduce bias.[19]

Plating Efficiency (PE, eqn (7)) and Surviving Fraction (SF. eqn (8)) were calculated to evaluate the effects of Curc-GNPs and radiation treatment on PC-3 cells. PE was determined as the ratio of the number of colonies formed to the number of cells originally seeded. This metric reflects the proportion of cells capable of adhering to the plate and forming colonies following GNP exposure. SF was calculated to determine the proportion of cells that retained their ability to form colonies after exposure to radiation treatment. Data were fitted to the linear–quadratic (LQ) model (eqn (9)) *via* non-linear regression using *Python 3.11* (*curve_fit* in *SciPy* 1.15 and *NumPy 2.1*). This yielded best-fit values for $\alpha$ (the linear cell-killing coefficient) and $\beta$ (the quadratic cell-killing coefficient), along with the corresponding standard errors, the dose for 50% effect $D_{50}$, and the sensitizer enhancement ratio (SER, eqn (10)).

$$\mathrm{PE} = \left(\frac{\text{Number of colonies}}{\text{Number of cells seeded}}\right) \times 100\% \quad (7)$$

$$\mathrm{SF} = \left(\frac{\text{Number of colonies after radiotherapy}}{\text{Number of cells seeded} \times \mathrm{PE}}\right) \times 100\% \quad (8)$$

$$S(D) = \mathrm{e}^{-\alpha D - \beta D^2} \quad (9)$$

$$\mathrm{SER} = \frac{D_{50}\text{ with GNP}}{D_{50}\text{ without GNP}} \quad (10)$$

### 2.7 Statistical analysis

All experiments were carried out in at least triplicates to report mean values with ± standard errors. The statistical method used for measuring *p*-values was the paired *t*-test (2 groups) and the ANOVA (3 or more groups). *P*-values mentioned are relative to the control unless otherwise stated in the text.

## 3. Results and discussion

### 3.1 Colloidal stability

The synthesized Curc-GNP solution exhibited a ruby red color, which is characteristic of spherical gold nanoparticles. Curcumin functioned as both the reducing agent and stabilizing ligand, simplifying the synthesis process significantly compared to conventional methods, which typically require separate reducing and stabilizing agents. Traditionally, compounds such as sodium borohydride ($NaBH_4$), hydrazine, or ascorbic acid serve as reducing agents, while separate stabilizing agents like polyethylene glycol (PEG) or cetyltrimethylammonium bromide (CTAB) are introduced subsequently to prevent nanoparticle aggregation. Utilizing curcumin as a dual-functional reducing agent simplifies the synthesis procedure, eliminates the necessity of toxic reagents, and enhances biocompatibility.[6,20]

Table 1 Curc-GNP characterization and stability test. (A) The mean diameter, (B) PDI, and (C) zeta potential of Curc-GNPs incubated at 37 °C in different media for 48 hours

| | $T = 0$ | 24 h | 48 h |
|---|---|---|---|
| | **(A) Diameter (nm)** | | |
| Curc-GNP in water | 20.8 ± 2.3 | 22.0 ± 2.3 | 22.4 ± 2.1 |
| Curc-GNP in RPMI | 23.8 ± 2.8 | 146 ± 19 | 840 ± 80 |
| Curc-GNP in RPMI + FBS | 38 ± 6 | 35 ± 6 | 36 ± 7 |
| | **(B) PDI** | | |
| Curc-GNP in water | 0.13 ± 0.01 | 0.13 ± 0.01 | 0.14 ± 0.02 |
| Curc-GNP in RPMI | 0.18 ± 0.02 | 0.19 ± 0.02 | 0.58 ± 0.07 |
| Curc-GNP in RPMI + FBS | 0.26 ± 0.02 | 0.30 ± 0.02 | 0.29 ± 0.03 |
| | **(C) Zeta potential (mV)** | | |
| Curc-GNP in water | −33.9 ± 2.2 | −36.2 ± 2.3 | −35.3 ± 2.5 |
| Curc-GNP in RPMI | −13 ± 8 | −12 ± 7 | −13 ± 6 |
| Curc-GNP in RPMI + FBS | −5 ± 8 | −5 ± 6 | −4 ± 6 |

To investigate the impact of serum proteins on nanoparticle stability, colloidal stability tests were conducted under different media conditions (Table 1). Curc-GNP solutions demonstrated excellent stability in ultrapure water, as evidenced by consistent hydrodynamic diameters (20 to 22 nm), stable polydispersity indices (PDI < 0.2), and zeta potentials (−33.91 to −36.18 mV) throughout the 48 hour testing period. In serum-supplemented RPMI, Curc-GNPs maintained reasonable stability, though there was a notable increase in hydrodynamic size (~35 nm) and PDI (0.28) within 48 hours compared to water alone (Fig. S1†). UV-vis spectroscopy consistently revealed characteristic peaks at approximately 525 nm, indicating maintained colloidal stability of Curc-GNPs in serum-supplemented RPMI (Fig. 2A). Here, serum proteins help stabilize Curc-GNPs through corona formation, despite increasing particle size and reducing zeta potential.[21] On the other hand, Curc-GNPs in RPMI without FBS exhibited a significant increase in diameter (839.8 nm) and PDI (0.579) accompanied by a red shift of the characteristic peak in the UV-vis spectra over time, indicative of nanoparticle aggregation (Fig. 2B). Visually, the colloidal suspension of Curc-GNPs in RPMI without FBS was more opaque compared to those in serum-supplemented RPMI and water, confirming the formation of aggregates (Fig. S2†). The protein corona is a very important design parameter for all nanodrug delivery systems as it can greatly influence biodistribution and pharmacokinetics. Our Curc-GNP structure contains an outer layer of curcumin which is hydrophobic and is reported to have strong affinity and binding interactions with serum albumin.[22] The beneficial role of albumin-mediated GNP delivery includes enhanced circulation time, low toxicity, and selective accumulation in tumor tissues.[23,24]

### 3.2 Surface characterization & curcumin loading

The TEM analysis shows the morphology and the size distribution of the dehydrated Curc-GNPs (Fig. 3A), which has a mean

 

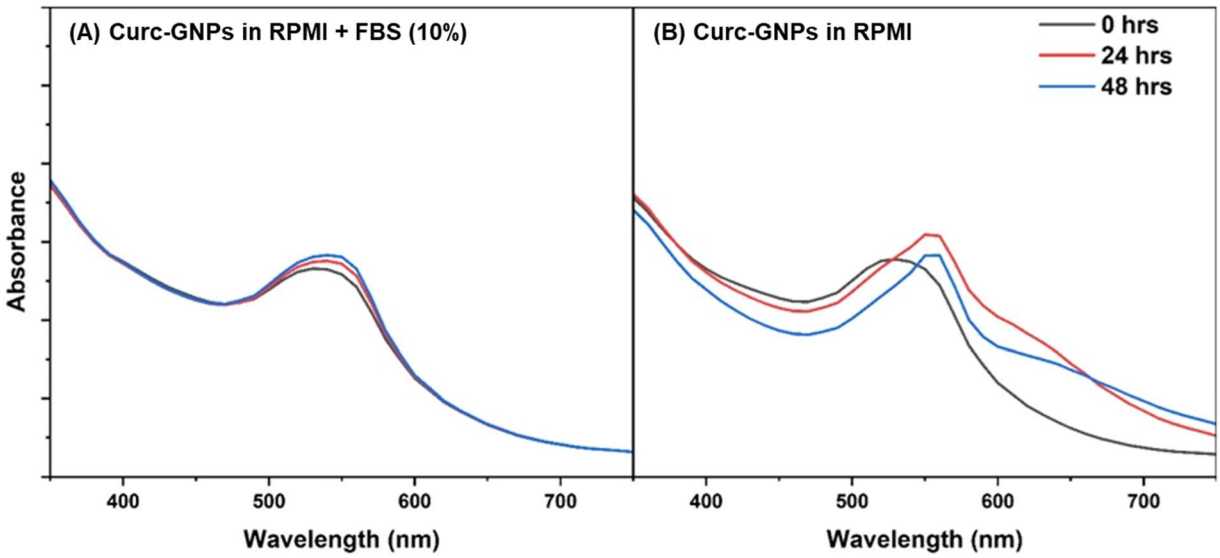


Fig. 2 UV-vis spectra of Curc-GNPs in (A) serum-supplemented RPMI and (B) serum-free RPMI at 0, 24, and 48 hours.

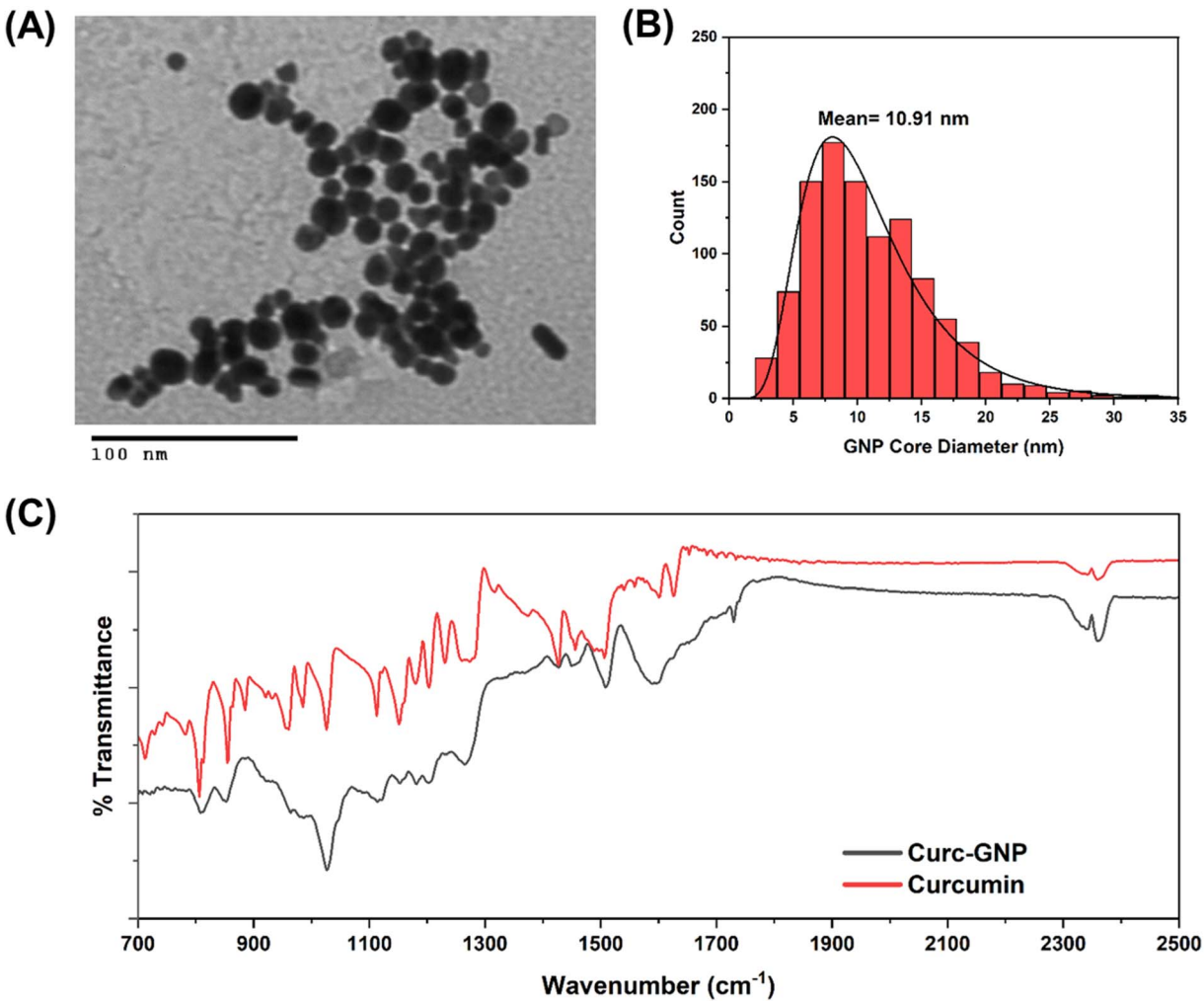


Fig. 3 Surface characterization of Curc-GNPs. (A) TEM image of Curc-GNP. (B) Size distribution of Curc-GNP's Au cores. (C) FTIR spectra of Curc-GNP (black) and curcumin (red).

diameter of 11 nm ± 5, representing the size of the core of Curc-GNPs (Fig. 3B). Since the mean hydrodynamic diameter of Curc-GNPs was ~20 nm in ultrapure water (Table 1), we can deduce the thickness of the curcumin coating and hydration layer around the GNP core is approximately ~5 nm on each side. In the case of serum-supplemented media, the protein corona resulted in an increase in the hydrodynamic diameter by 10–15 nm.

FTIR spectra (Fig. 3C) of curcumin alone showed a strong, conjugated carbonyl (C=O) stretch near 1625–1628 $cm^{-1}$ that overlaps with aromatic C=C signals. Upon binding to GNPs, this band diminished in intensity and partially shifted to a higher frequency around 1700–1740 $cm^{-1}$. This upward shift suggests that curcumin's β-diketone moiety was converted to a less hydrogen-bonded carbonyl, consistent with coordination to the gold surface. Conversely, the aromatic ring vibrations around 1500–1600 $cm^{-1}$ remained largely unaltered, indicating that the phenyl rings do not participate directly in binding with GNPs. Additionally, a notable decrease or disappearance of the enolic =C–OH bending peak near 960 $cm^{-1}$ further supports the involvement of the β-diketone/enol functional group in anchoring curcumin to the gold surface. Altogether, these spectral changes confirm that curcumin was successfully coated onto the GNPs primarily *via* its polar β-diketone/enol while the aromatic rings remain structurally intact.

The HPLC method exhibited strong linearity for curcumin standards in the range of 0.1–54.25 μg $mL^{-1}$, with an $R^2$ value of 0.996. Standard measurements between 5.425 and 54.25 μg $mL^{-1}$ were especially accurate as they all yielded % deviations of less than 5% of expected value (Fig. 4C). Curcumin consistently eluted at approximately 4.03 ± 0.01 minutes for all samples analyzed, including both standards and Curc-GNP desorbate (Fig. 4A and B). The first desorption cycle yielded an average curcumin concentration of 7.011 ± 0.014 μg $mL^{-1}$. As the solution was diluted 10-fold for HPLC analysis, the actual supernatant concentration was 70.11 μg $mL^{-1}$. With a total supernatant volume of 25 mL, this corresponds to 1.75 mg of

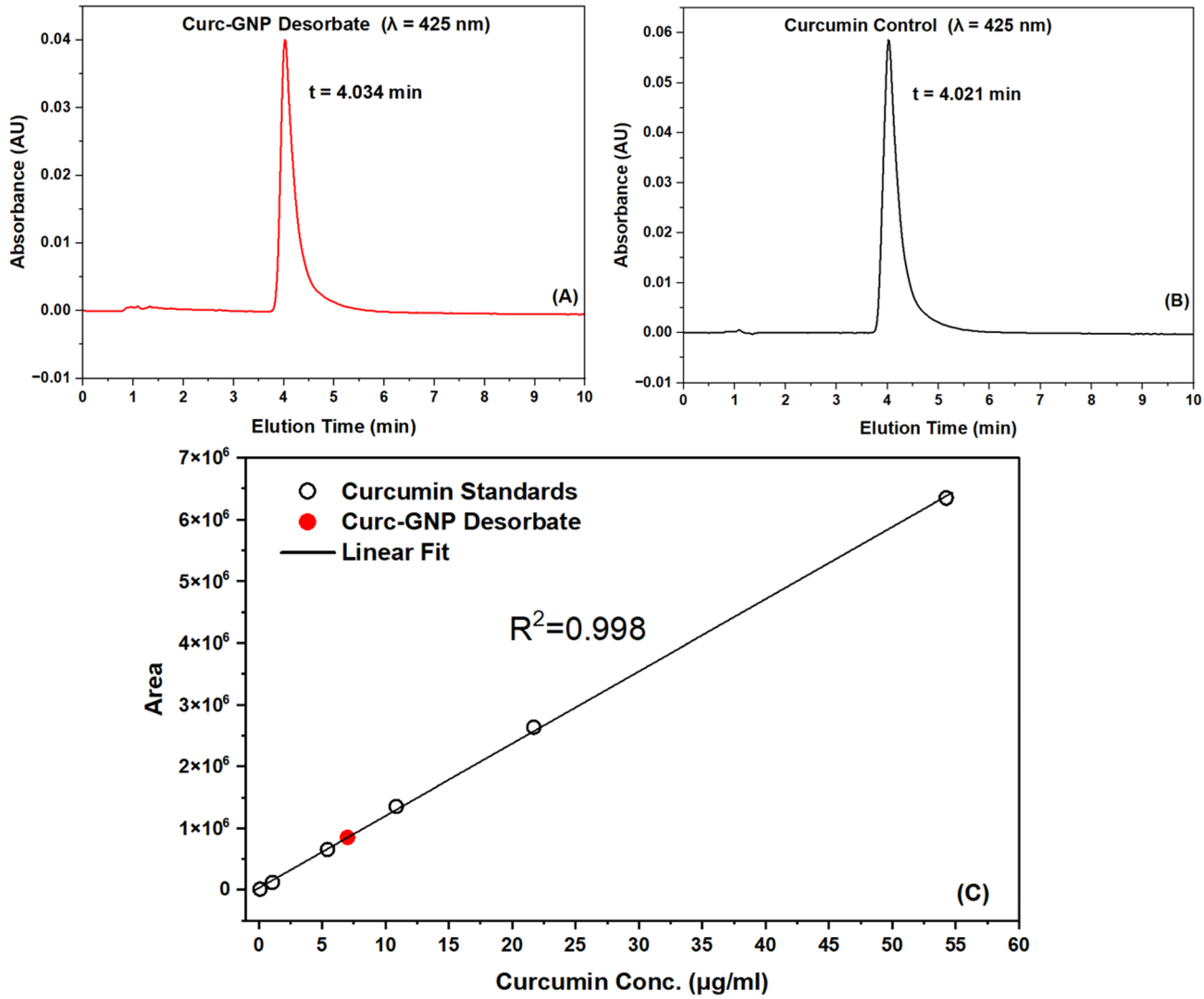


Fig. 4 HPLC analysis of curcumin loading. (A) Chromatogram of Curc-GNP desorbate ($t$ = 4.034 min). (B) Chromatogram of curcumin control ($t$ = 4.02 min). (C) Calibration curve for curcumin (0.1–55 μg $mL^{-1}$; $R^2$ = 0.998) with Curc-GNP desorbate plotted in red.

curcumin recovered. A second desorption cycle was performed to capture any remaining curcumin on the GNPs however, the measured value was extremely small <0.5 μg $mL^{-1}$, below the quantification limit of 1 ppm. Thus, it can be concluded that the first desorption cycle removed >97% of the curcumin from the GNPs, demonstrating the effectiveness of the acidic ethanol method. ICP analysis of the resuspended pellet revealed a gold concentration of 336.54 ± 0.12 μg $mL^{-1}$, equivalent to 8.41 mg of gold in the 25 mL suspension. Using eqn (1), the curcumin loading is calculated as follows:

$$\omega_{Curc} = \frac{m_{Curc}}{m_{Au}} = \frac{1.75\ mg}{8.41\ mg} = 0.208\ mg\ Curcumin\ per\ mg\ Au$$

This corresponds to a curcumin loading of 20.8 wt%. The Curc-GNP synthesis initially used 9.21 mg of curcumin, so the 1.75 mg detected on the GNPs represents a ~19% encapsulation efficiency. Quantification of curcumin loading on GNPs is crucial, as curcumin is the active therapeutic agent. Accurate loading data provide essential context for interpreting *in vitro* results in terms of therapeutic efficacy. Furthermore, precise quantification ensures reproducibility and facilitates comparison between different formulations.

### 3.3 Antioxidant potential

Curcumin is recognized as a potent antioxidant, with numerous studies confirming its efficacy in both bulk and nanoparticle forms.[7–9,20] The antioxidant activity is largely attributed to its unique chemical structure, which includes carbon–carbon double bonds, phenyl rings with hydroxyl and *O*-methoxy groups, and a β-diketo group that serves as an active site for chemical reactions (Fig. 5A). The aromatic rings with hydroxyl groups can donate electrons or hydrogen atoms to neutralize free radicals, while the stability of the molecule is maintained by the aromatic structure.[20,25]

The DPPH assay is a widely utilized method for assessing the radical scavenging ability of GNPs. Previous studies have demonstrated elevated DPPH scavenging ability of various surface-modified GNPs.[26,27] In our experiment, we employed quercetin as a positive control alongside Cit-GNPs, which are the standard and most frequently cited GNPs in the literature.[11] Both Cit-GNPs and Curc-GNPs exhibited a dose-dependent increase in DPPH inhibition; however, at higher concentrations, the increase in inhibition appeared to plateau (Fig. 5B). Notably, Curc-GNPs exhibited a 2.1 ($p \approx 0.003$) and 1.43-fold ($p \approx 0.07$) higher DPPH inhibition than Cit-GNPs at the lowest (25 μg $mL^{-1}$) and highest (200 μg $mL^{-1}$) concentrations respectively.

### 3.4 Cytotoxicity of Curc-GNPs in PC-3 cells

In our study, we employed the XTT assay to evaluate the cytotoxicity of Curc-GNPs on PC-3 cells at three incubation time points: 24, 48, and 72 hours. Curc-GNPs exhibited a biphasic dose–response relationship, with cell viability remaining high across the 0–100 μg $mL^{-1}$ concentration range and decreasing sharply from 100–1000 μg $mL^{-1}$ at all three time points (Fig. 6). Moreover, the rate of cell death was much higher at the higher concentrations (500–1000 μg $mL^{-1}$) (Fig. S3†). At 24 hours, the viability was 112.75% ± 2.06 at 100 μg $mL^{-1}$ ($p < 0.05$), 89.48% ± 7.72 at 200 μg $mL^{-1}$ ($p < 0.05$), 72.58% ± 5.26 at 500 μg $mL^{-1}$ ($p < 0.01$), and 58.06% ± 6.41 at 1000 μg $mL^{-1}$ ($p < 0.001$) (Fig. 6A). The increase in viability at lower concentrations (25–100 μg $mL^{-1}$) may indicate a protective effect that promotes cell proliferation, warranting further mechanistic investigation. These findings suggest that lower concentrations of Curc-GNPs are not inherently toxic to prostate cancer cells *in vitro*.

Several mechanisms may explain curcumin's protective effect at low concentrations. Curcumin is a radical scavenger that modulates ROS levels, thereby effectively quenching ROS species within PC3 cells, and its anti-inflammatory effects may further promote cell viability. However, beyond a certain threshold, oxidative stress may overwhelm protective pathways, leading to cell injury or death.[28] Hence, the biphasic dose–response attributed to an optimal balance between curcumin's anti-inflammatory action and its influence on proliferation

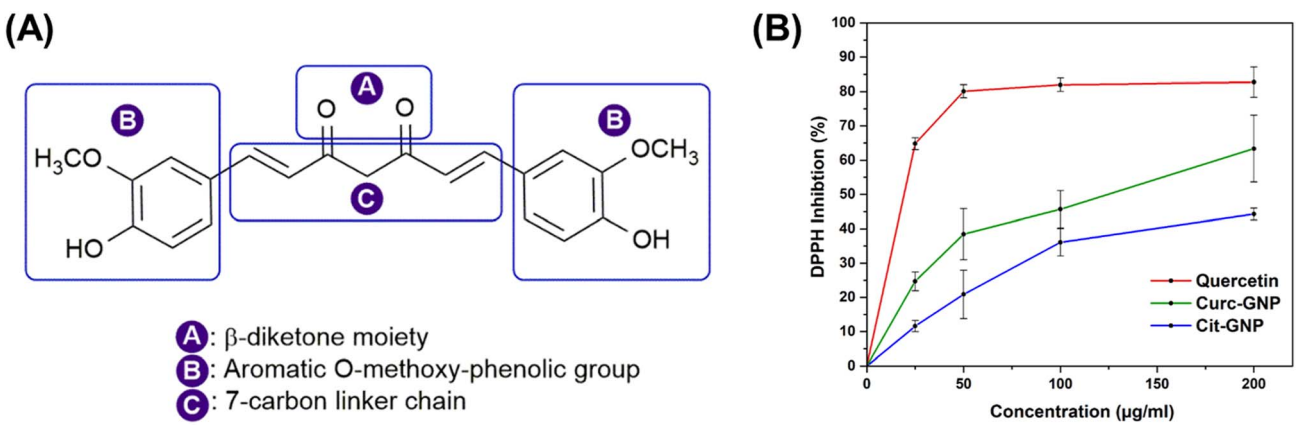


Fig. 5 Antioxidant activity of Curc-GNPs. (A) The chemical structure of curcumin, which includes a diketone moiety, two aromatic ring systems, and a seven-carbon linker chain. (B) DPPH inhibition of Curc-GNP compared to Cit-GNP and quercetin (positive control) at varying concentrations (25–200 μg $mL^{-1}$).

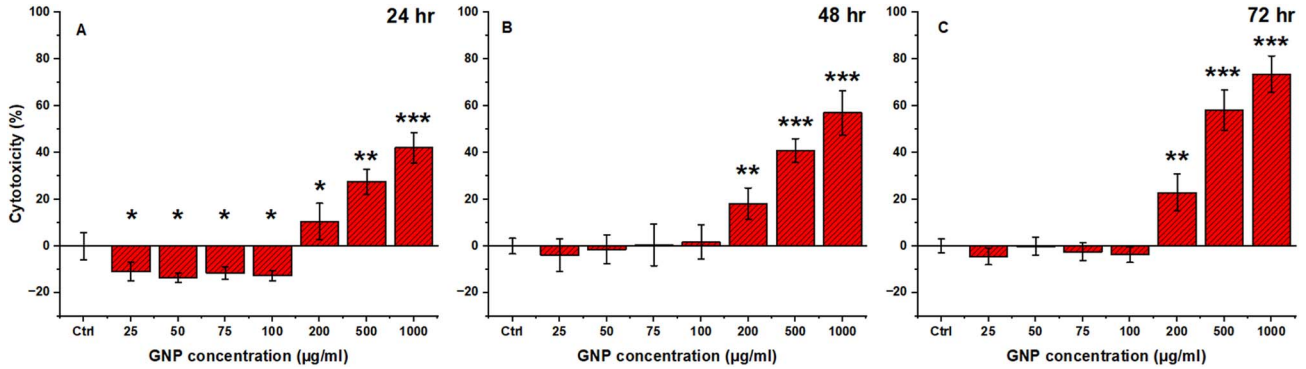


Fig. 6 XTT cytotoxicity assay. Cytotoxicity of Curc-GNPs in RPMI + FBS with PC-3 cells for (A) 24 h (B) 48 h and (C) 72 h incubation periods. The statistical significance was indicated by *$p < 0.05$, **$p < 0.01$, and ***$p < 0.001$.

markers.[28–30] To our knowledge, no one has reported a hormetic response in relation to *in vitro* or *in vivo* GNP studies.

Our results show that curcumin could be stimulating PC-3 cells at low doses and induce apoptosis at high doses. This biphasic effect is well-documented in literature.[29,31,32] For example, MDA-MB breast cancer cells exhibited increased glutathione (GSH) levels (138% $P < 0.01$) at low curcumin concentrations, but strong inhibition (−56% $P < 0.01$) at concentrations above 25 mg $L^{-1}$.[31] Vashisht *et al.* treated buffalo granulosa cells with various concentrations of curcumin-loaded exosomes and observed increased expression of cell proliferation markers and anti-inflammatory signals at low concentrations (10–20 μM). These included a reduction in pro-inflammatory cytokines such as IL-1β, IL-6, and TNF-α.[29] In our study, further investigation is needed to clarify the mechanisms underlying the biphasic hormetic response of Curc-GNPs. We postulate that threshold-dependent events may determine whether curcumin acts protectively *via* antioxidant effects or triggers apoptosis. For example, the activation of caspase cascades or the loss of mitochondrial membrane potential may serve as critical thresholds that shift the cellular response from survival to cell death. Future work should examine cell signaling and gene expression to better understand the biphasic effects of Curc-GNPs on PC-3 cells.

### 3.5 Curc-GNP uptake in PC3 cells

The primary mechanisms of GNP uptake in PC3 cells are endocytosis and pinocytosis. Endocytosis is a well-characterized process where the cell membrane invaginates to form an intracellular vesicle, facilitating nanoparticle internalization, especially for functionalized GNPs.[33] Pinocytosis, on the other hand, is a non-specific process involving the uptake of surrounding extracellular fluid and solutes, which may also contribute to the internalization of GNPs in PC3 cells.[33,34] With these two mechanisms in mind, we investigated the interaction between Curc-GNPs and PC3 cells by incubating two different concentrations of Curc-GNPs (50 or 100 μg $mL^{-1}$) in PC3 cells with or without 10% FBS for 10 and 24 hours at 37 °C. The results showed that longer incubation time (24 hours) resulted in significantly higher uptake compared to shorter incubation times (10 hours), a trend that was consistent across both medium conditions ($p < 0.05$) (Fig. 7). Additionally, higher Curc-GNP concentration (100 μg $mL^{-1}$) led to an increased uptake compared to that of lower concentration (50 μg $mL^{-1}$), which was also statistically significant in both medium conditions ($p < 0.05$).

Interestingly, serum-supplementation had a notable impact on GNP uptake, with lower uptake observed across both incubation times compared to non-serum-supplemented medium. This effect was most pronounced at 24 hours, where the cellular uptake in non-serum-supplemented medium (72.38 pg per cell ± 15.14) was 3.52-fold higher than that of serum-supplemented medium (20.59 pg per cell ± 3.83) ($p < 0.001$), suggesting that the absence of serum proteins may enhance nanoparticle–cell interactions by preventing protein corona formation. With no serum proteins adhered to the surface of Curc-GNPs, the bare curcumin coating can directly bind with the lipid-rich PC-3 membrane, leading to an increased uptake of Curc-GNPs in a non-serum-supplemented medium. Additionally, the elevated Au detected in our PC3 cell study may be partially driven by Curc-GNP aggregation in a non-serum-supplemented medium as shown in the stability study (Table 1), leading to the settling of larger GNPs onto PC-3 cells. The findings from our *in vitro* Curc-GNP uptake study highlight the importance of nanoparticle drug design that accounts for protein interactions in the serum-rich *in vivo* settings. Under physiological conditions, nanoparticles may acquire a biomolecular corona composed of albumin, immunoglobulins, apolipoproteins, and complement factors.[35,36] This corona can sterically hinder direct ligand–receptor contact, or may alter cell signaling interactions that ultimately reduce cellular recognition and internalization. For example, nanoparticle-bound immunoglobulins can trigger opsonization and clearance by the mononuclear phagocyte system, leading to accumulation in the liver and spleen.[35] The serum-free conditions highlight the optimal cell-association potential of the curcumin coating and inform future surface engineering strategies of Curc-GNPs, such as stealth PEGylation or pre-adsorption of circulatory enhancing proteins.[36]

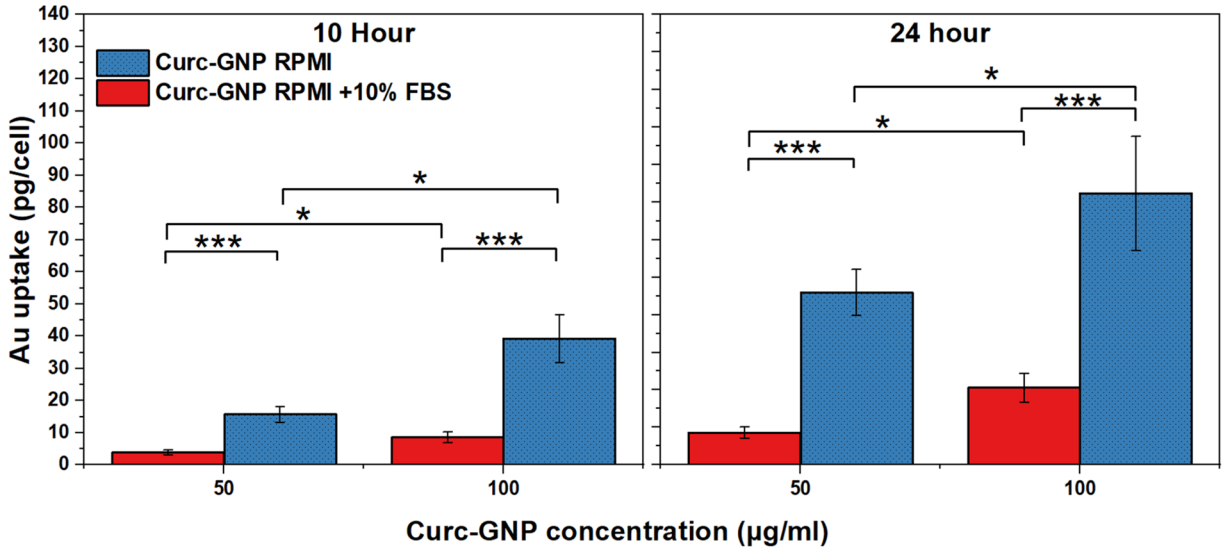


Fig. 7 Cellular uptake of Curc-GNPs. The concentration of Au detected in PC3 cells after incubating with Curc-GNPs at two different concentrations (50 and 100 μg $mL^{-1}$) in two different medium conditions (RPMI with or without 10% FBS) for 10 and 24 hours at 37 °C. The statistical significance was indicated by *$p < 0.05$, **$p < 0.01$, and ***$p < 0.001$.

### 3.6 Radiosensitization enhancement

Several radiosensitization studies have demonstrated the radio-enhancing effects of functionalized GNPs in prostate cancer.[11,12,37] Once localized in the cells, GNPs distributed near the nucleus and within cytoplasmic structures contributed to enhanced DNA damage and impaired repair mechanisms.[38]

Herein, we initially revealed a dose-dependent increase in radiotherapy-induced cell death of Curc-GNPs *via* the clonogenic assay (Fig. 8A). At the lowest concentration (25 μg $mL^{-1}$), the sensitizer enhancement ratio (SER) was 0.979 corresponding to a 2.1% decrease from the control group (0 μg $mL^{-1}$), indicating an insufficient ability to enhance radiation sensitivity compared to the control group (Table 2). This may reflect a transient radioprotective effect, potentially due to curcumin's antioxidant properties, which could scavenge radiation-induced ROS at low concentrations. This finding is consistent with our cytotoxicity study (Fig. 6), which indicated enhanced cell viability at sub-toxic Curc-GNP concentrations. On the other hand, with Curc-GNPs at 50 μg $mL^{-1}$ and above, the SER values increased with respect to Curc-GNPs, which correlated with the radiotherapy-induced cell death (Fig. 8A).

Further insights into the radiosensitizing mechanisms were provided by the Linear–Quadratic (LQ) model. The $\alpha$ parameter, which represents single-track lethal DNA damage and ROS-mediated cell death, exhibited a steep increase with Curc-GNP concentration (Table 2). This suggests that Curc-GNP enhances ROS-mediated cytotoxicity, likely driven by the photoelectric effect, wherein X-ray irradiation of gold atoms results in the release of secondary electrons, thereby amplifying radiation-induced damage.[13] In contrast, the $\beta$ parameter, associated with double-track sublethal DNA damage and complex lesion repair, changed marginally and showed no link to Curc-GNP concentration. This observation indicates that the primary mechanism of enhanced cell killing is ROS-induced oxidative stress caused by Curc-GNPs rather than an enhancement of direct DNA strand breaks. Additionally, there was a progressive decrease in $D_{50}$ with increasing Curc-GNP concentrations, from 2.094 Gy at 25 μg $mL^{-1}$ to 1.127 Gy at 500 μg $mL^{-1}$. This trend indicates that higher Au concentrations significantly lower the radiation dose required for equivalent therapeutic efficacy. Notably, curcumin is a well-documented inhibitor of the NF-κB pathway, which plays a critical role in cancer cell survival, inflammation, and radioresistance. Upon irradiation, NF-κB is typically activated, promoting the expression of anti-apoptotic genes (Bcl-3, XIAP) that counteract radiation-induced damage.[39] Curcumin's ability to suppress NF-κB activation can sensitize tumor cells to radiotherapy by diminishing these survival signals and enhancing apoptotic susceptibility. Furthermore, curcumin is known to cause cell cycle arrest at G2/M phase, a phase where cells are intrinsically more radiation sensitive due to highly condensed chromatin, and limited ability to repair DNA.[3–5,9] By synchronizing a larger proportion of cells in this radiosensitive phase, curcumin loading on GNPs amplifies radiation-induced DNA damage. Previous reports in prostate and colorectal cancer cells have shown that curcumin-induced G2/M arrest correlates with increased γ-H2AX foci and reduced clonogenic survival following irradiation.[4,10]

Colony formation assays (Fig. 8B) illustrate a clear reduction in colony number with increasing Curc-GNP concentration and radiation dose. The most pronounced effect was observed horizontally (increasing Curc-GNP concentration) rather than vertically (increasing radiation dose), indicating that Curc-GNPs primarily enhance radiosensitivity rather than directly inhibiting proliferation. Morphological changes were evident with increasing radiation doses; colonies at 0 Gy were large and circular, while those at 6 Gy appeared smaller, irregularly shaped, or reduced to faint specks.

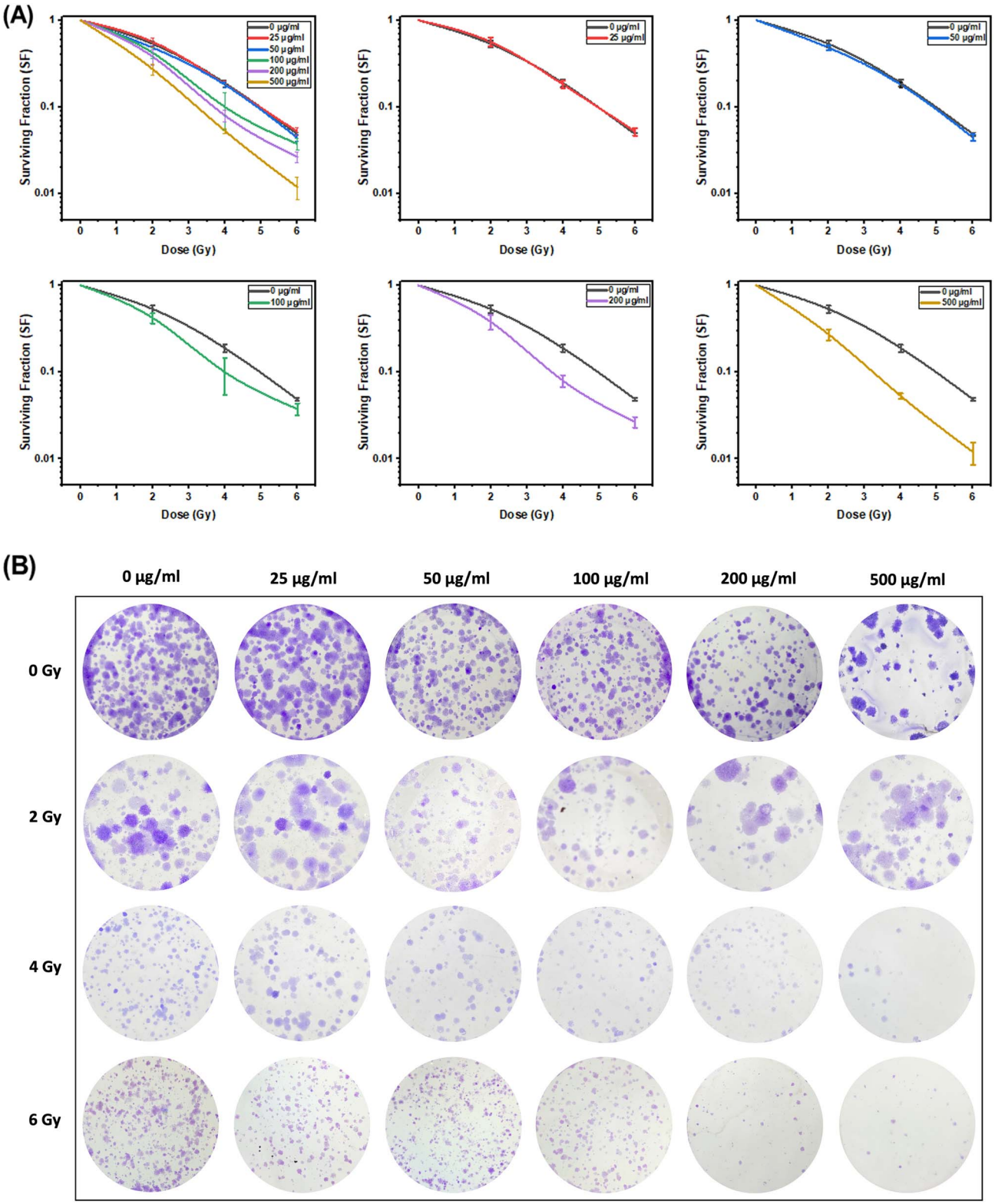


Fig. 8 The radiosensitization analysis. (A) The clonogenic assay and (B) colony formation assay showing the concentration-dependent (0–500 μg $mL^{-1}$) cell death of PC3 cells *via* Curc-GNP-mediated radiotherapy. Viable cells are indicated in violet.

Table 2 The changes in $\alpha$ (the linear cell-killing coefficient), $\beta$ (the quadratic cell-killing coefficient), $D_{50}$, SER, and the $\alpha/\beta$ ratio at varying Curc-GNP concentrations

| Concentration | $\alpha$ | $\beta$ | $D_{50}$ | SER | $\alpha/\beta$ |
|---|---|---|---|---|---|
| 0 μg mL$^{-1}$ | 0.173 | 0.04 | 2.05 | 1 | 4.325 |
| 25 μg mL$^{-1}$ | 0.24 | 0.044 | 2.094 | 0.979 | 5.454545 |
| 50 μg mL$^{-1}$ | 0.311 | 0.032 | 1.87 | 1.097 | 9.71875 |
| 100 μg mL$^{-1}$ | 0.343 | 0.052 | 1.623 | 1.263 | 6.596154 |
| 200 μg mL$^{-1}$ | 0.341 | 0.068 | 1.554 | 1.319 | 5.014706 |
| 500 μg mL$^{-1}$ | 0.579 | 0.032 | 1.127 | 1.82 | 18.09375 |

# 4. Conclusion

In this study, we systematically characterized and evaluated Curc-GNPs as radiosensitizers targeting prostate cancer cells. Our colloidal stability tests demonstrated that Curc-GNPs maintained excellent dispersion in serum-supplemented medium but formed aggregate under serum-free conditions, an effect partly attributed to protein corona formation. Curc-GNPs showed superior antioxidant activity compared to conventional Cit-GNPs, reflecting the inherent free-radical–scavenging properties of curcumin. Cytotoxicity analyses revealed a biphasic dose response where low Curc-GNP concentrations slightly enhanced cell viability, whereas high concentrations (>100 μg mL$^{-1}$) elicited a pronounced cytotoxic effect. Subsequent uptake studies indicated that serum-free conditions and prolonged incubation maximize Curc-GNP internalization, likely due to direct curcumin-cell membrane interactions and aggregation of Curc-GNPs. Critically, clonogenic assays demonstrated robust radiosensitization, in which SER increased in a concentration-dependent manner, peaking at 1.82 in cells treated with 500 μg per mL Curc-GNPs plus ionizing radiation. Mechanistically, our data indicate that Curc-GNP-mediated radiosensitization is largely governed by an increased $\alpha$-parameter in the linear–quadratic model, signifying enhanced ROS production *via* photoelectric interactions between gold and X-rays. For translation of Curc-GNPs to *in vivo* models, challenges surrounding their biphasic dose response must be clarified, particularly the underlying mechanisms and the identification of a therapeutic dose window. Further surface engineering is recommended to mitigate serum protein adhesion and prevent aggregation in protein-poor, acidic tumor microenvironments. Strategies such as PEGylation or pre-adsorption with select proteins should be explored. Lastly, to more accurately quantify *in vivo* radiosensitization and enhance therapeutic efficacy, converting Curc-GNPs into a radiopharmaceutical formulation (Curc-$^{198}$GNP) *via* neutron activation represents a logical next step.

# Abbreviations

The following abbreviations are used in this manuscript:

| | |
|---|---|
| Cit-GNP | Citrate-coated gold nanoparticles |
| CTAB | Cetyltrimethylammonium bromide |
| Curc-GNP | Curcumin-coated gold nanoparticles |
| DPPH | 2,2-Diphenyl-1-picrylhydrazyl |
| FBS | Fetal bovine serum |
| FTIR | Fourier transform infrared spectroscopy |
| GNP | Gold nanoparticle |
| ICP-MS | Inductively coupled plasma-mass spectrometry |
| LOQ | Limit of quantification |
| LQ | Linear–quadratic |
| MDL | Method detection limit |
| NF-κB | Nuclear factor kappa B |
| PDI | Polydispersity index |
| PE | Plating efficiency |
| PEG | Polyethylene glycol |
| PNC | Penicillin streptomycin |
| ROS | Reactive oxygen species |
| SER | Sensitizer enhancement ratio |
| SF | Surviving fraction |
| TEM | Transmission electron microscopy |

# Data availability

The authors confirm that the data supporting the findings of this study are available within the article and its ESI.†

# Author contributions

Conceptualization, M. A., S. W., E. O.; methodology, M. A., S. W.; software, M. A.; validation, M. A., M. A. A.; formal analysis, M. A., S. W., E. O.; investigation, M. A., M. M. A.; resources, S. W., E. O.; data curation, M. A.; writing—original draft preparation, M. A.; writing—review and editing, M. A., M. M. A.; visualization, M. A.; supervision, S. W., E. O.; project administration, S. W., E. O.; funding acquisition, S. W., E. O. All authors have read and agreed to the published version of the manuscript.

# Conflicts of interest

There are no conflicts of interest to declare.

# Acknowledgements

This research was funded by the Telus Ride for Dad Foundation (S. W.), MITACS (S. W., E. O.). The authors gratefully acknowledge Dr Faten Salim and the staff of the Analytical Lab, Department of Chemical Engineering, University of Waterloo, for their valuable assistance.

# References

1 P. Rawla, Epidemiology of Prostate Cancer, *World J. Oncol.*, 2019, **10**(2), 63, DOI: 10.14740/wjon1191.
2 D. J. Herr, *et al.*, Outcomes after definitive radiation therapy for localized prostate cancer in a national health care delivery system, *Cancer*, 2023, **129**(20), 3326–3333, DOI: 10.1002/cncr.34916.
3 A. B. Kunnumakkara, *et al.*, Curcumin Sensitizes Human Colorectal Cancer Xenografts in Nude Mice to γ-Radiation

by Targeting Nuclear Factor-κB–Regulated Gene Products, *Clin. Cancer Res.*, 2008, **14**(7), 2128–2136, DOI: 10.1158/1078-0432.CCR-07-4722.

4 D. Chendil, *et al.*, Curcumin confers radiosensitizing effect in prostate cancer cell line PC-3, *Oncogene*, 2004, **23**(8), 1599–1607, DOI: 10.1038/sj.onc.1207284.

5 J. Rutz, *et al.*, Growth, Proliferation and Metastasis of Prostate Cancer Cells Is Blocked by Low-Dose Curcumin in Combination with Light Irradiation, *Int. J. Mol. Sci.*, 2021, **22**(18), 9966, DOI: 10.3390/ijms22189966.

6 S. Nambiar, *et al.*, Synthesis of curcumin-functionalized gold nanoparticles and cytotoxicity studies in human prostate cancer cell line, *Appl. Nanosci.*, 2018, **8**(3), 347–357, DOI: 10.1007/s13204-018-0728-6.

7 J. S. Sharifi-Rad, Y. E. Rayess, A. A. Rizk, C. Sadaka, R. Zgheib, W. Zam and N. Martins, Turmeric and Its Major Compound Curcumin on Health: Bioactive Effects and Safety Profiles for Food, Pharmaceutical, Biotechnological and Medicinal Applications, *Front. Pharmacol*, 2020, **11**, 550909, DOI: 10.3389/fphar.2020.01021.

8 V. Verma, Relationship and interactions of curcumin with radiation therapy, *World J. Clin. Oncol.*, 2016, **7**(3), 275, DOI: 10.5306/wjco.v7.i3.275.

9 V. Zoi, *et al.*, Radiosensitization and Radioprotection by Curcumin in Glioblastoma and Other Cancers, *Biomedicines*, 2022, **10**(2), 312, DOI: 10.3390/biomedicines10020312.

10 S. K. Sandur, *et al.*, Curcumin Modulates the Radiosensitivity of Colorectal Cancer Cells by Suppressing Constitutive and Inducible NF-κB Activity, *Int. J. Radiat. Oncol., Biol., Phys.*, 2009, **75**(2), 534–542, DOI: 10.1016/j.ijrobp.2009.06.034.

11 M. I. Anik, *et al.*, Gold nanoparticles (GNPs) in biomedical and clinical applications: A review, *Nano*, 2022, **3**(4), 792–828, DOI: 10.1002/nano.202100255.

12 V.-K. Nguyen, *et al.*, Gold Nanoparticle-Enhanced Production of Reactive Oxygen Species for Radiotherapy and Phototherapy, *Nanomaterials*, 2025, **15**(4), 317, DOI: 10.3390/nano15040317.

13 D. Howard, S. Sebastian, Q. V.-C. Le, B. Thierry and I. Kempson, Chemical Mechanisms of Nanoparticle Radiosensitization and Radioprotection: A Review of Structure-Function Relationships Influencing Reactive Oxygen Species, *Int. J. Mol. Sci.*, 2020, **21**(2), 579, DOI: 10.3390/ijms21020579.

14 J. Dong, *et al.*, Synthesis of Precision Gold Nanoparticles Using Turkevich Method, *KONA Powder Part. J.*, 2020, **37**, 224, DOI: 10.14356/kona.2020011.

15 İ. Gülçin, Antioxidant properties of resveratrol: A structure–activity insight, *Innovative Food Sci. Emerging Technol.*, 2010, **11**(1), 210–218, DOI: 10.1016/j.ifset.2009.07.002.

16 Roche Diagnostics GmbH, Cell Proliferation Kit II (XTT) – Product information sheet (Version 19). Roche, 2021, Retrieved from, https://www.sigmaaldrich.com.

17 C. Carnovale, *et al.*, Identifying Trends in Gold Nanoparticle Toxicity and Uptake: Size, Shape, Capping Ligand, and Biological Corona, *ACS Omega*, 2019, **4**(1), 242–256, DOI: 10.1021/acsomega.8b03227.

18 N. A. P. Franken, *et al.*, Clonogenic assay of cells in vitro, *Nat. Protoc.*, 2006, **1**, 2315–2319, DOI: 10.1038/nprot.2006.339.

19 *Colony Counter*, 2017, Retrieved from.

20 S.-In Sohn, *et al.*, Biomedical Applications and Bioavailability of Curcumin—An Updated Overview, *Pharmaceutics*, 2021, **13**(12), 2102, DOI: 10.3390/pharmaceutics13122102.

21 E. Casals, *et al.*, Time Evolution of the Nanoparticle Protein Corona, *ACS Nano*, 2010, **4**(7), 3623–3632, DOI: 10.1021/nn901372t.

22 A. Barik, *et al.*, Photophysical Studies on Binding of Curcumin to Bovine Serum Albumin, *Photochem. Photobiol.*, 2003, **77**(6), 597–603, DOI: 10.1562/0031-8655(2003)0770597PSOBOC2.0.CO2.

23 M. R. Green, *et al.* Abraxane®, a novel Cremophor®-free, albumin-bound particle form of paclitaxel for the treatment of advanced non-small-cell lung cancer, *Ann. Oncol.*, 2006, **17**(8), 1263–1268, DOI: 10.1093/annonc/mdl104.

24 Na Qu, *et al.*, Albumin Nanoparticle-Based Drug Delivery Systems, *Int. J. Nanomed.*, 2024, **19**, 6945, DOI: 10.2147/IJN.S467876.

25 M. Platzer, *et al.*, Radical Scavenging Mechanisms of Phenolic Compounds: A Quantitative Structure-Property Relationship (QSPR) Study, *Front. Nutr.*, 2022, **9**, 882458, DOI: 10.3389/fnut.2022.882458.

26 S. R. Chavva, *et al.*, Epigallocatechin Gallate-Gold Nanoparticles Exhibit Superior Antitumor Activity Compared to Conventional Gold Nanoparticles: Potential Synergistic Interactions, *Nanomaterials*, 2019, **9**(3), 396, DOI: 10.3390/nano9030396.

27 F. Fayazbakhsh, *et al.*, Evaluating the antioxidant potential of resveratrol-gold nanoparticles in preventing oxidative stress in endothelium on a chip, *Sci. Rep.*, 2023, **13**, 21344, DOI: 10.1038/s41598-023-47291-6.

28 N. S. A. Moghaddam, *et al.*, Hormetic effects of curcumin: What is the evidence?, *J. Cell. Physiol.*, 2019, **234**(7), 10060–10071, DOI: 10.1002/jcp.27880.

29 M. Vashisht, *et al.*, Curcumin primed exosomes reverses LPS-induced pro-inflammatory gene expression in buffalo granulosa cells, *J. Cell. Biochem.*, 2018, **119**(2), 1488–1500, DOI: 10.1002/jcb.26309.

30 J. Wendt, *et al.*, Are Supra-Physiological Plant-Based Antioxidants Ready for the Clinic? A Scoping Review of Hormetic Influences Driving Positive Clinical Outcomes, *Glob. Adv. Integr. Med. Health*, 2024, **13**, 27536130241231508, DOI: 10.1177/27536130241231508.

31 M. Bayet-Robert and D. Morvan, Metabolomics Reveals Metabolic Targets and Biphasic Responses in Breast Cancer Cells Treated by Curcumin Alone and in Association with Docetaxel, *PLoS One*, 2013, **8**(3), e57971, DOI: 10.1371/journal.pone.0057971.

32 N. S. A. Moghaddam, *et al.*, Hormetic effects of curcumin: What is the evidence?, *J. Cell. Physiol.*, 2019, **234**(7), 10060–10071, DOI: 10.1002/jcp.27880.

33 B. D. Chithrani and W. C. W. Chan, Elucidating the Mechanism of Cellular Uptake and Removal of Protein-

Coated Gold Nanoparticles of Different Sizes and Shapes, *Nano Lett.*, 2007, **7**(6), 1542–1550, DOI: **10.1021/nl070363y**.

34 E. Bilgi, D. A. Winkler and C. Oksel Karakus, Identifying factors controlling cellular uptake of gold nanoparticles by machine learning, *J. Drug Targeting*, 2024, **32**(1), 66–73, DOI: **10.1080/1061186X.2023.2288995**.

35 Y. Li, L. Saba, R. I. Scheinman, N. K. Banda, M. Moghimi and D. Simberg, Nanoparticle-Binding Immunoglobulins Predict Variable Complement Responses in Healthy and Diseased Cohorts, *ACS Nano*, 2024, **18**(42), 28649–28658, DOI: **10.1021/acsnano.4c05087**.

36 M. Li, *et al.*, Nanoparticle elasticity affects systemic circulation lifetime by modulating adsorption of apolipoprotein A-I in corona formation, *Nat. Commun.*, 2022, **13**(4137), 1–16, DOI: **10.1038/s41467-022-31882-4**.

37 X. Zhang, *et al.*, Enhanced radiation sensitivity in prostate cancer by gold-nanoparticles, *Clin. Invest. Med.*, 2008, **31**(3), 160–167, DOI: **10.25011/cim.v31i3.3473**.

38 I. Tremi, *et al.*, Biological Response of Human Cancer Cells to Ionizing Radiation in Combination with Gold Nanoparticles, *Cancers*, 2022, **14**(20), 5086, DOI: **10.3390/cancers14205086**.

39 S. J. Veuger, *et al.*, Ionizing radiation-induced NF-κB activation requires PARP-1 function to confer radio-resistance, *Oncogene*, 2008, **28**(6), 832, DOI: **10.1038/onc.2008.439**.